The use of MPM to estimate the behaviour of rigid structures during landslides

Gonzalez Acosta, Leon; Vardon, Phil; Hicks, Michael; Pantev, Ivaylo

Publication date
2018

Document Version
Final published version

Published in
Proceedings of the 9th European Conference on Numerical Methods in Geotechnical Engineering (NUMGE 2018)

Citation (APA)
Gonzalez Acosta, L., Vardon, P., Hicks, M., & Pantev, I. (2018). The use of MPM to estimate the behaviour of rigid structures during landslides. In M. de Matos Fernandes (Ed.), *Proceedings of the 9th European Conference on Numerical Methods in Geotechnical Engineering (NUMGE 2018): June 25-27, 2018, Porto, Portugal* (Vol. 1). (Numerical Methods in Geotechnical Engineering IX,; Vol. 9, No. 1). CRC Press. https://www.taylorfrancis.com/books/9780429446931/chapters/10.1201/9780429446931-81

Important note
To cite this publication, please use the final published version (if applicable).
Please check the document version above.

Numerical Methods in Geotechnical Engineering IX – Cardoso et al. (Eds)
© 2018 Taylor & Francis Group, London, ISBN 978-1-138-33198-3

The use of MPM to estimate the behaviour of rigid structures during landslides

L. González Acosta, I. Pantev, P.J. Vardon & M.A. Hicks
Section of Geo-Engineering, Faculty of Civil Engineering and Geosciences, Delft University of Technology, Delft, The Netherlands

ABSTRACT: In geotechnical engineering, proper design of retaining structures is of great importance, since failure of these structures can lead to catastrophic consequences. Nowadays, the finite element method is seen as a reliable numerical technique to analyze soil behaviour and is widely used to assess the interaction between soil and rigid structures. However, a disadvantage of this method is the difficulty of simulating contact between separate bodies. Because of this, the event of a slope failing and colliding with a rigid body cannot be analyzed, so that the additional forces acting against the rigid body caused by the motion of the ground are neglected. With the recent development of the Material Point Method (MPM), this limitation has been overcome and problems involving large deformation and multiple bodies in contact can be analyzed. In this paper, the effect of a landslide colliding with a rigid wall has been studied, and multiple initial conditions have been considered in order to identify the critical case.

1 INTRODUCTION

During the early years of geotechnical engineering, the only methods available to assess the stability of rigid retaining structures (retaining walls, sheet piles, etc.) were those related with limit equilibrium. The biggest disadvantage of such methods is their inability to take account of the complexity of the problem; for example, with respect to the geometry, construction stages, material behavior, variability of soil properties, and irregular loading conditions.

Years later, with the implementation of numerical techniques such as the finite element method (FEM) and the finite difference method (FDM), taking account of complexities in geotechnical analysis has become more feasible. Using these techniques, it is now possible to compute the stability and interaction between the soil and rigid structures, returning important information for the design process. Moreover, in the particular case of retaining structures, FEM has proven to be appropriate for solving this type of problem under both static (Hosseinzadeh & Joosse, 2015) and dynamic (Gazetas et al. 2016) loading conditions. However, because the connectivity between the mesh and domain is essential for most standard FEM analyses, there is a limit to the range of problems that can be solved with the method.

During the last 20 years, new numerical techniques such as mesh free and meshless methods have been developed, to eliminate the need of using a continuum mesh to simulate the material. Among these techniques, the material point method (Sulsky et al. 1994, 1995) has been proven to solve problems with satisfactory results. Since, in MPM, the material is not attached to the mesh, large deformations can be simulated, enabling the analysis of complex geotechnical problems such as a progressive slope failures (Wang et al. 2016) and landslides (Soga et al. 2016). Moreover, due to the development of a contact detection algorithm (Bardenhagen et al. 2000, 2001), the interaction between separate bodies is feasible, so that the simulation of a landslide impacting on a retaining wall has become possible.

In the first part of this paper, the background of MPM and the contact detection algorithm are outlined, followed by the analysis of an elastic body bouncing on a rigid surface to demonstrate the efficiency and accuracy of the formulation. Finally, the analysis of a slope colliding with a rigid body is performed, including a parametric study to find the critical conditions.

2 THEORETICAL FORMULATION

2.1 *MPM background*

A great advantage of MPM over other mesh free and meshless techniques is its significant overlap with FEM, albeit with two key differences. The first difference is that material properties are attached to the material points and not to the elements;

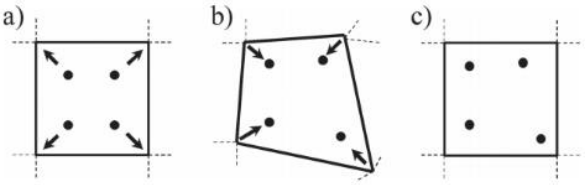

Figure 1. MPM solution steps: a) mapping phase, b) solution of momentum balance at the nodes, and c) convection phase.

the second difference is that, after the equations of motion have been solved at the nodes and the mesh is distorted, the material points adopt their new positions and the mesh is reset to its original position. Figure 1 illustrates the MPM solution procedure. Firstly, particle variables such as mass, momentum, velocity and stresses are mapped to the nodes; next the momentum equation is solved for the velocities and accelerations at the nodes; then, the updated solution is transferred to the material points by mapping the nodal values using shape functions; and finally, the mesh is reset.

Since MPM shares similarities with the FEM mechanics framework (Chen et al. 2015), the weak form of the momentum conservation is given as

$$\int_{\Omega} \rho \mathbf{a} \cdot \delta u dV + \int_{\Omega} \rho \boldsymbol{\sigma} \nabla \cdot \delta u dV = \int_{\Omega} \rho \mathbf{b} \cdot \delta u dV + \int_{\Gamma} \rho \boldsymbol{\tau}^{s} \cdot \delta u dA \tag{1}$$

where ρ is the material density, $\mathbf{a}$ the acceleration, δu the virtual displacement, V the body volume, $\boldsymbol{\sigma}$ the Cauchy stress, $\mathbf{b}$ the body forces, $\boldsymbol{\tau}^{s}$ the prescribed tractions, Γ the traction boundary, and Ω the solution domain.

Note that since the integration of internal and external forces, as well as kinematic variables, is performed considering the new positions of the material points, the oscillation of stresses, velocities, accelerations, and many other quantities is inevitable, reducing the accuracy of the results. However, an explanation of these matters is beyond the scope of this work.

2.2 *Contact detection*

Contact detection was developed in MPM to allow interaction between bodies (e.g. collision, penetration, sliding, and adhesion). To detect contact, the velocity field of a single body is compared to the velocity field accounting for all bodies in the system. Due to the discrete domain of the shape functions, these will only be different at the nodes where contact occurs, i.e. at those nodes with contributions from more than one body. The contact at the nodes is computed as

$$\mathbf{v}^{cm} - \mathbf{v}^{i} \neq 0 \tag{2}$$

where $\mathbf{v}^{cm}$ is the velocity field accounting for all bodies, and $\mathbf{v}^{i}$ is the body velocity field.

After contact is established, further behaviour, such as approach or departure, is computed by using the surface normal direction at every contact node, i.e.

$$\left(\mathbf{v}^{i} - \mathbf{v}^{cm}\right) \cdot \mathbf{n}^{i} > 0 \tag{3}$$

where

$$\mathbf{n}^{i} = \sum_{p=1}^{nmp} G_{ip} m_{p} \tag{4}$$

In which $\mathbf{n}^{i}$ is the body surface normal, *nmp* is the number of material points in the support elements, G_{ip} is the gradient of the shape function with respect to the position of the material point, and m_{p} is the material point mass.

Figure 2 gives an illustration of the contact nodes detected after the total velocity at the nodes diverges from the single body velocity contribution.

3 BENCHMARK PROBLEM

3.1 *Bouncing of a block*

To demonstrate the accuracy and performance of MPM with the contact algorithm, a benchmark

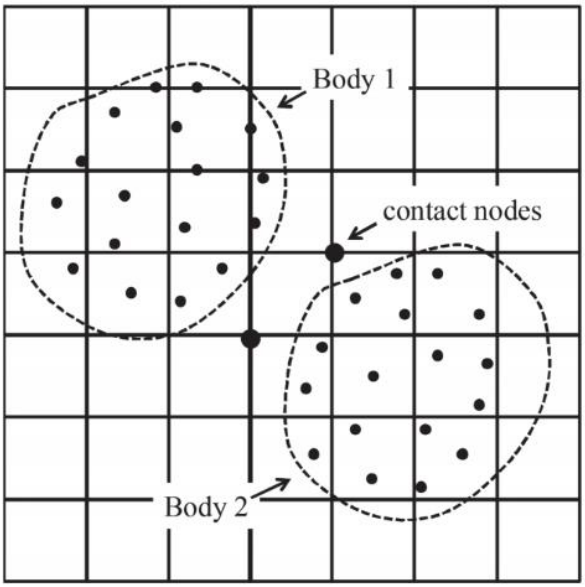

Figure 2. Contact detection nodes after mapping velocities on the background mesh.

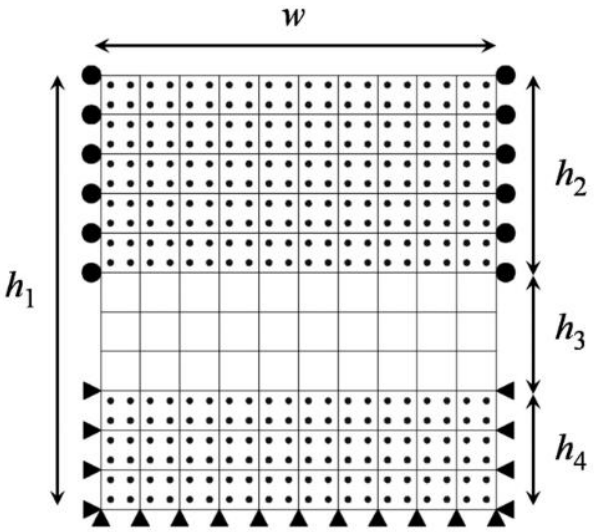

Figure 3. Collision between an elastic block and a rigid body.

problem has been analysed. Specifically, an elastic body is allowed to free fall, so that it collides with a second body acting as a rigid surface. The falling body is a block made up of 200 material points and it is dropped from a height of $h_3 = 0.30$ m relative to the second body representing the infinite rigid surface, which is composed of 120 material points. Figure 3 shows a sketch of the problem. As can be seen, the background mesh is made up of square elements of dimensions $\Delta x = \Delta y = 0.10$ m, and the material points are initially evenly spaced at $\xi = \pm 0.5$ and $\eta = \pm 0.5$ in terms of local coordinates. The total height of the domain is $h_1 = 1.1$ m, and the falling body and the rigid body have a height of $h_2 = 0.5$ m and $h_4 = 0.30$ m respectively. The width of the domain is $w = 1.0$ m.

The block and the rigid surface are considered as perfectly elastic bodies, both with an elastic modulus and Poisson's ratio of $E = 500$ kN/m^2 and $\nu = 0.49$ respectively. The reason for choosing such a high Poisson's ratio is to avoid high compression and deformation of the bodies during contact, thereby avoiding stress oscillation problems caused by the material points crossing element boundaries.

The boundary conditions for this problem are as follows. For the rigid surface, the nodes at the right, left and bottom are fixed in both directions to prevent any displacement. In contrast, the nodes at the right and left boundary for the falling block are fixed just in the horizontal direction, in order to allow free fall and avoid horizontal deformation. To consider the surface body as a rigid body with infinite stiffness, the displacements, velocities, and accelerations are erased after each step to prevent any distortion and the effects this can cause to the body representing the falling block. Finally, the initial velocity of the falling block is zero, and gravity is the only external force acting on it, whereas the body representing the rigid surface is not affected by gravity and is only affected by the forces developed during the contact.

3.2 *Results*

Figure 4 shows the analytical velocity at time t of a body bouncing over a surface, and the average velocity of all material points from the falling block bouncing over a second body considering two element sizes, $\Delta x = 0.1$ m and $\Delta x = 0.05$ m. As can be seen, the average velocity of both solutions matches the analytical one perfectly during free fall, but neither reaches the analytical maximum velocity. After two bounces, the maximum velocity reached reduces substantially. It is also evident that when using a smaller mesh, the solution is closer to the analytical solution, showing that the contact and body behavior depend on the mesh size. The main reason why the velocity of the free falling block does not reach the maximum analytical velocity, is that contact detection happens if the material points of both bodies are in neighboring elements, leading to an early bounce. The solution converges to the analytical one as the element size reduces.

In Figure 5, the average vertical position h of the falling body is plotted against time and compared with the analytical vertical position for a perfectly elastic body bouncing on a rigid surface. As before, the comparison is made using two different cell sizes. The position after bouncing for the analytical solution was computed using the analytical velocity after bouncing, leading to the perfect bounce that reaches the initial position.

As was seen in the previous figure, the computed results match the analytical solution closely during free fall, but the bounce occurs earlier. Also, after bouncing the block is unable to reach

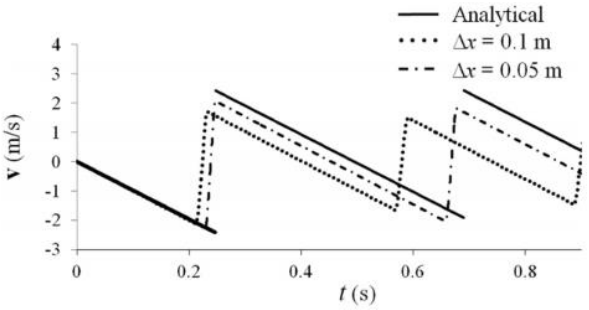

Figure 4. Analytical and experimental average velocities of material points of the falling body before and after bouncing.

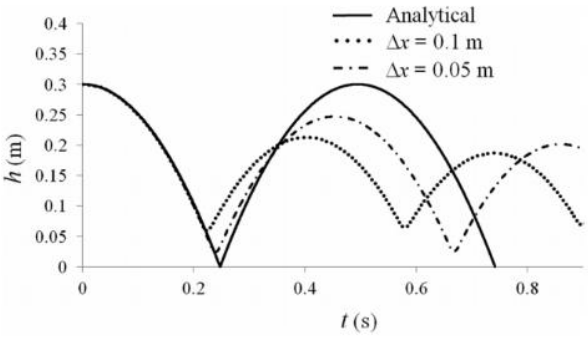

Figure 5. Analytical and experimental average vertical positions of the bouncing body with time.

the initial position, and this becomes more evident after the second bounce. As mentioned before, the reason why the body does not reach the rigid surface (h = 0 m), is because contact takes place at a distance of 1 element. Again, with the reduction of element size, the contact distance is smaller, leading to a solution closer to the analytical one. Finally, it is clear that the maximum altitude reached by the bouncing body is lower than the analytical solution because of energy losses. These are due to (i) the resetting of the rigid body, and (ii) stress oscillation in MPM.

The above analysis proves that the contact algorithm works properly and that interaction between bodies can be simulated with suitable results using MPM. For more information regarding the mathematical background of the contact algorithm, as well as benchmark problems to validate its use with MPM, the reader is directed to Pantev (2016).

4 GEOTECHNICAL APPLICATION

4.1 *Collision of a landslide with rigid structure*

To illustrate the application of the combined MPM and contact algorithm in geotechnical problems, the behavior of a rigid body when a landslide collides with it was analized. Figure 6 shows a sketch of the problem, which consists of 2 bodies. Body 1 (B_1) is a low strength block of soil that, after failure, collides with body 2 (B_2) representing a rigid wall. Both bodies are constructed using background meshes of size $\Delta x = \Delta y = 0.1$ m, and each element is initially filled with 4 and 9 material points for body 1 and body 2 respectively. The height of B_1 is h_1 = 2.0 m and its length is l_1 = 3.0 m, whereas the height of body 2 is h_2 = 1.0 m and its length is l_1 = 1.0 m. During this investigation, the distance (d) between the bodies is varied to find the distance at which the impact on B_2 is highest. Note that gravity only acts on B_1, and that the bottom nodes

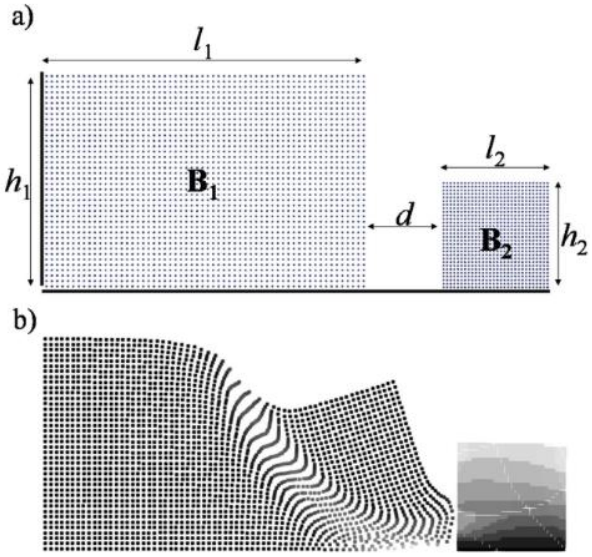

Figure 6. a) Sketch of the problem, and b) final configuration including displacement contours in rigid body.

of B_2 are fixed in both directions to avoid a potential slide or roll-over of the body after impact.

The soil making up body 1 has a peak cohesion of c_p = 6 kPa, a residual cohesion of c_r = 1.5 kPa, a softening modulus of s_m = -15 kPa, an elastic modulus of E = 1000 kPa, and a Poisson's ratio of ν = 0.30. Body 2 is purely elastic, with an elastic modulus of E = 2000 kPa and a Poisson's ratio of ν = 0.49. The friction coefficient acting between the soil and the bottom boundary, and between the soil and the rigid body, is μ = 1.0, so that after contact the material sticks to the rigid body. To quantify the reaction in body 2, the mean value of the deviatoric stress (q) was computed based on the 9 points in the base element, in which the reaction is bigger. The stresses in body 1 and body 2 are computed using CMPM as in Gonzalez et al. (2017), rather than using classical MPM, in order to have more accurate results, especially for body 2 which develops high stresses due to the incompressibility caused by the high Poisson's ratio.

4.2 *Results*

Figure 7 shows that the critical distance (i.e. the distance at which the reaction in body 2 is highest) is d_c = 0.5 m, whereas for d = 0.2 and 1.5 m the reactions are similar. The reason for similar values at d = 0.2 and 1.5 m is because at these values the velocity of the landslide is similar and small; in the first case, it is because failure has not fully developed in body 1, so that the velocity of the body has not increased significantly, whereas in the second case the body has completely failed but the velocity developed has started to decrease because the

travel distance of the slide is longer. Note that the collision times for the different analyses are different because the distance d is different; hence, the measure of the deviatoric stress is computed relative to the time of the collision (t_c) and not before.

Figure 8 illustrates the configuration of the landslide at the critical condition, as well as the collision at the maximum distance (in which the effect of the impact is smaller).

After the critical distance was found, another set of analyses were performed for $d = d_c$, in order to investigate the influence of the properties of body 1 on the stresses built up in body 2. The property that is varied is the residual cohesion, with values of c_r = 1.5, 2.0, 2.5 and 3.0 kPa. As in the previous analysis, the change in the residual cohesion affects the behavior of body 1, as well as causing the contact to occur at different times for each analysis. As before, the time from the moment of collision was used to plot the results.

Figure 9 shows that the highest deviatoric stresses are generated when the residual cohesion of body 1 is the smallest, and that, with an increase of the residual cohesion, the impact on body 2 decreases. Clearly, if the residual cohesion is small, the forces resisting the displacement of body 1 are smaller, leading to a more sudden failure that will cause the development of higher velocities and thereby a bigger impact with the rigid body.

Finally, the mesh size effect has been analyzed, using the critical distance d_c and the critical residual cohesion of c_r = 1.5 kPa. Specifically, four analyses are performed considering mesh sizes of Δx = 1/10, 1/8, 1/6, and 1/4 m.

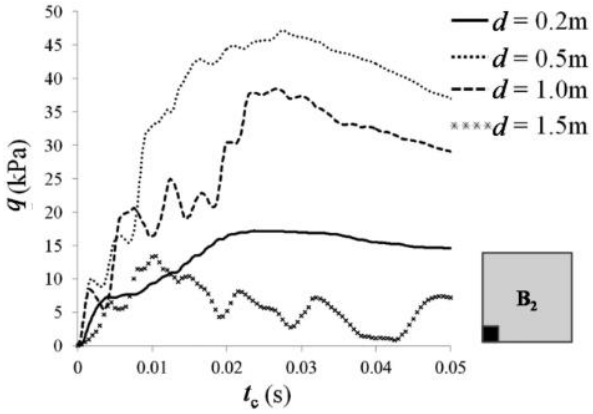

Figure 7. Mean deviatoric stress evolution with time at the base of body 2 as a function of initial distance between the bodies.

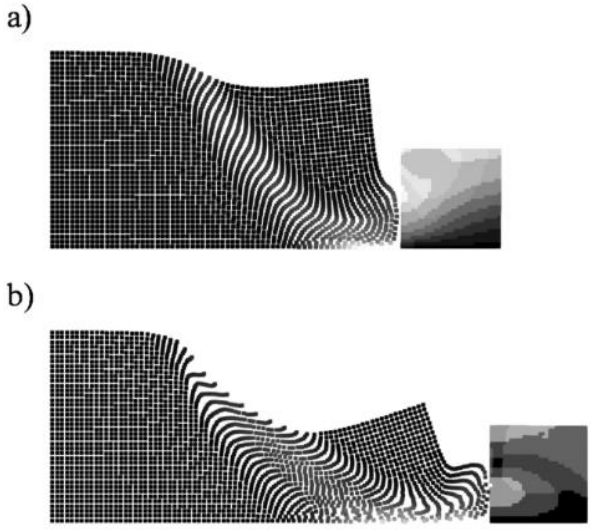

Figure 8. Landslide collision a) at the critical distance, and b) at the maximum distance.

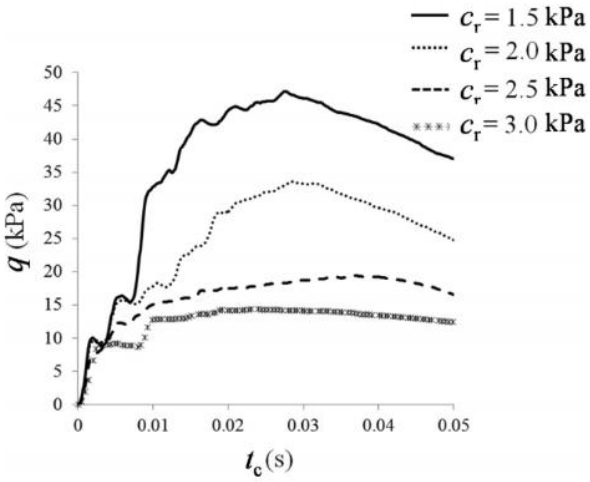

Figure 9. Deviatoric stress in body 2 considering different residual cohesion values for body 1.

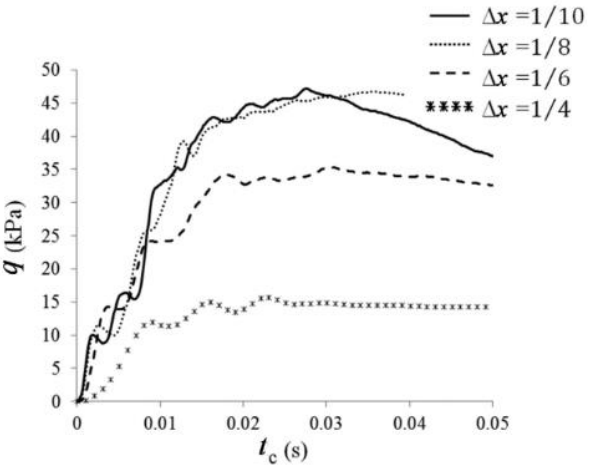

Figure 10. Deviatoric stress in body 2 for different mesh sizes.

As can be seen in Figure 10, the maximum deviatoric stress is reached when the mesh size is smallest, and this is thought to be mainly a consequence of no strain regularization induced in the current verison of the algorithm. Hence, for a smaller element size, the shear band in B_1 is narrower and the slope failure more sudden, causing an increase in the velocity of the slide and a greater impact on B_2.

5 CONCLUSIONS

This paper has investigated the performance of MPM with a contact algorithm to analyse the behaviour of a rigid structure during impact from a landslide, considering the variation of the mechanical properties of the sliding material and the initial conditions of the problem.

The results have shown that the contact algorithm in MPM is suitable for determining if bodies are interacting or not. Also, the transfer of information between bodies in contact has been demonstrated, although improvements are needed in the computation of the normal direction at the boundary of the bodies, since this can severely impact the accuracy of the analysis. The oscillations in the solution caused by material points moving between elements during contact is also a significant problem that causes an irregular redistribution of the contact forces, especially if contact is maintained over a longer time.

The results are an indication that MPM is an appropriate tool for analysing geotechnical problems. Considering a broad combination of initial conditions and a range of mechanical properties, it is possible to obtain a wide range of results in order to detect the most critical scenario.

REFERENCES

Bardenhagen, S.G., Brackbill, J.U., & Sulsky, D. 2000. The material-point method for granular materials. *Computer Methods in Applied Mechanics and Engineering 187(3–4)*: 529–541.

Bardenhagen, S.G., Guilkey, J.E., Roessig, K.M., Brackbill J.U., & Foster J.C. 2001. An improved contact algorithm for the material point method and application to stress propagation in granular material. *Computer Modeling in Engineering and Sciences 2(4)*: 509–522.

Chen, Z.P., Qiu, X.M., Zhang, X., & Lian, Y.P. 2015. Improved coupling of finite element method with material point method based on a particle-to-surface contact algorithm. *Computer Methods in Applied Mechanics and Engineering 293*: 1–19.

Gazetas, G., Garini, E., & Zafeirakos, A. 2016. Seismic analysis of tall anchored sheet-pile walls. *Soil Dynamics and Earthquake Engineering 91*: 209–221.

Gonzalez Acosta, L., Vardon, P.J., & Hicks, M.A. 2017. Composite material point method (CMPM) to improve stress recovery for quasi-static problems. *Procedia Engineering 175*: 324–331.

Hosseinzadeh, S., & Joosse, J.F. 2015. Design optimization of retaining walls in narrow trenches using both analytical and numerical methods. *Computers and Geotechnics 69*: 338–351.

Pantev, I. 2016. Contact modelling in the material point method. *MSc thesis, Delft University of Technology,* 2016.

Soga, K., Alonso, E., Yerro, A., Kumar, K., & Bandara, S. 2016. Trends in large-deformation analysis of landslide mass movements with particular emphasis on the material point method. *Géotechnique 66(3)*: 248–273.

Sulsky, D., Chen, A., & Schreyer H.L. 1994. A particle method for history dependent materials. *Computer Methods in Applied Mechanics & Engineering 118(1–2)*: 179–196.

Sulsky, D., Zhou, S., & Schreyer H.L. 1995. Application of a particle-in-cell method to solid mechanics. *Computer Physics Communications 87(1)*: 236–252.

Wang, B., Vardon, P.J., & Hicks, M.A. 2016. Investigation of retrogressive and progressive slope failure mechanisms using the material point method. *Computers and Geotechnics 78*: 88–98.